Rev. Roum. Sci. Techn.– Électrotechn. et Énerg.
Vol. **68**, *3*, pp. 317–322, Bucarest, 2023

MAGNETIC FIELD CONTROL IN AN ANALYTIC PLATFORM FOR ASSESSMENT OF PATHOGENIC BACTERIA

ALIN ALEXANDRU DOBRE[1], ALINA MONICA ILIE-SANDOIU[2], ALEXANDRU MIHAIL MOREGA[1], EUGEN GHEORGHIU[3,4]

Keywords: Magnetic actuation; Pathogen detection; Magnetic field; Numerical simulation.

The paper presents a conceptual, analytical platform with various pathogen detection applications based on a hybrid magnetic field source comprised of permanent magnets and solenoid coils fixed on the same magnetic yoke that acts as a magnetic flux concentrator. The magnetic field creates magnetization forces that guide functionalized paramagnetic microparticles through the volume of an analyte sample to capture targeted pathogens. The presence of bacteria is sensed with an additional electrical impedance spectroscopy (EIS) module attached to the system at high-frequency electrical fields. The magnetic field control is studied using mathematical modeling and numerical simulation in several geometry setups, coil excitation, and remanent flux density values.

1. INTRODUCTION

In recent years, accentuated by the COVID-19 pandemic, there has been an increased demand for devices capable of quickly and on-site detecting different biomarkers that would determine a much faster, efficient, and accurate clinical diagnosis, still in the early stages of the disease, thus so that the drug treatment has the best possible effectiveness. Various detection methods, such as methods based on polymerase chain reaction (PCR), which determine the amplification of DNA samples, optical methods based on fluorometric detection of biological macromolecules and proteins, electrostatic methods [1], as well as methods based on electrochemical impedance spectroscopy, various genetic and microbial pathologies can be diagnosed and detected, such as periodontitis [2], cancer, different microbial and viral strains, *etc*., or they can be used to perform various toxicological tests [3] quickly.

Detection limits vary from a few cells to several million cells per ml of sample substance [4]. New studies show a lower detection limit, as low as 10^2 cells/ml. However, the detection time can take several hours [5]. Thus, recent studies have focused on improving detection methods and times, the additional costs associated with using various chemical compounds and reagents, the size of the reaction molecules, and the reduction of waste resulting from the process.

Among all the detection methods mentioned, the electrochemical detection method stands out, through which, together with MEMS (microelectromechanical systems) technology, various devices are developed, platforms that combine the detection capabilities of biosensors with electrical detection techniques, mechanical and even magnetic, if we refer to the use of magnetic particles to interact with the target cells, captured, from biological samples [6–15] or superparamagnetic particles, and together with electrical impedance spectroscopy, the analysis can be carried out quantitative of electrical quantities by using the reactions that take place at the level of the reaction surface of the microfluidic channels.

The molecular interactions at the level of the electrodes, which act as a reaction surface, allow the attachment of the target biological samples, and the use of superparamagnetic particles enables the improvement of the reaction and capture of the substance. Various signals are applied at different frequencies, after which the movements of the magnetic particles are analyzed. They move and attach to the reactive surface, once due to the flow of the fluid through the microchannel but also due to the magnetic field and the oscillations of the magnetic particles; particle formations provide information regarding the concentration of the analyzed substance. Thus, fluidic devices that combine sensing capabilities with fluid flow capabilities and sensing methods vary by application.

In this paper, we present the conceptual on-site device that combines sensing capabilities with magnetic stirring capabilities of biomarkers, intending to speed up detecting faster and more efficient biomarkers for accurate clinical diagnosis of usage in the early stages of the disease. Magnetic beads (MB) that can immobilize recognition elements (*e.g*., antibodies) via chemical linkers on their surface are used here as recognition elements to capture the target analyte.

The numerical model presented refers to the parametric study of the influence of the magnetic field on MB clusters, such as variations of the remanent magnetic flux density, $\mathbf{B}_{rem}$, for a fixed value of the excitation current, but also a specific $\mathbf{B}_{rem}$ and different values of the excitation current. The distance from the tank where the aggregate is located to the permanent magnets is also analyzed for a particular value of the remanent magnetic flux density.

Besides the detection method presented in this work, there are several other analytical detection methods based on the influence of the magnetic field, each having applicability for different types of sensors [12, 13]. Complementary to these detection methods, numerically, it has been established that the detection range varies between 100 bacteria/mL and 10^5 bacteria/mL [14].

This apparatus models the magnetic field actuation detailed in [6, 15], which is to relate the concentration of bacterial cells to the amplitude of the oscillating displacement of magnetic beads (MB)–bacteria complexes (MB clusters) within a sample when applying a periodic, oscillatory actuation field. The MB cluster oscillations can measured via electrical impedance assays. The electrical impedance spectroscopy part is not addressed here.

Section 2 presents the concept, section 3 provides for the mathematical model, and section 4 is devoted to the numerical simulation results and discussion. The conclusions are stated in the final section.

2. THE APPARATUS CONCEPT

MB with smaller diameters (500 nm, 200 nm, and 100 nm) were tested in the preliminary steps of assay development.

[1] The National University of Science and Technology, The Faculty of Electrical Engineering, Bucharest, Romania.
[2] The National University of Science and Technology, The Faculty of Medical Engineering, Bucharest, Romania.
[3] The International Centre of Biodynamics, Bucharest, Romania; [4] University of Bucharest, The Faculty of Biology, Bucharest, Romania.
E-mails: alin.dobre@upb.ro, alina.sandoiu@gmail.com , amm@iem.pub.ro, egheorghiu@biodyn.ro

DOI: 10.59277/RRST-EE.2023.68.3.12

Still, the number required to give a measurable signal must be more significant than the number of cells. Moreover, they also exhibited clustering without a target analyte and were thus susceptible to showing false positive results. An effective capturing yield and a high response at low target cells were noticed for 1 μm and 2.7 μm MB. Sizes smaller or larger than 1–3 μm were considered unsuitable for the application, as problems such as nonspecific clustering or clogging could occur.

Figure 1 presents the conceptual apparatus. The capsule that contains a fluidic suspension of the analyte sample and the magnetizable beads is placed within the free space between the poles of an electromagnet. The two coils on the specially shaped magnetic core produce the underlying magnetic field. The dc currents that power them are switched periodically to change the magnetic field direction, as presented in Fig. 4.

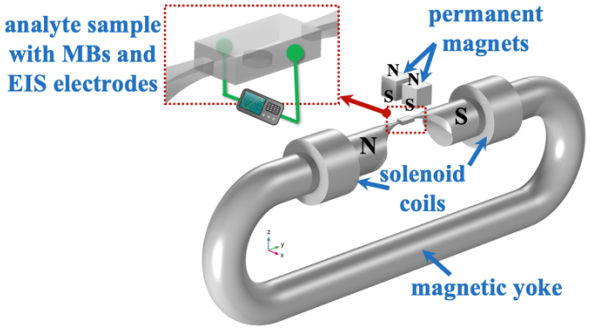

Fig. 1 – The analytic platform for the assessment of pathogens – a concept.

Switching the magnetic field orientation drives the aggregate into a (mainly) 1D left-right motion. This may facilitate and enhance their interception of the hopefully existing relevant biomarkers within the cell.

The permanent magnets placed above the cell produce a second magnetic field. Unlike the electromagnet field, the permanent magnets' field is highly non-uniform at the cell level. Therefore, provided that the apparatus design purposely emphasizes their effect, the magnetic forces and torques produced by the permanent magnets may significantly influence the beads' motion. A certain lifting effect is expected, thus reducing the possible friction that could occur in the beads' displacement concerning the bottom surface of the cell for beads of micrometric size.

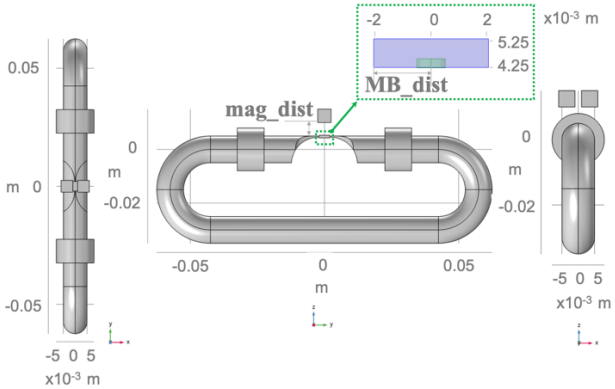

Fig. 2 – The dimensions of the detection platform and the geometric parameters considered in the study.

Several design parameters are worth considering for optimally sizing the apparatus: the electromagnet gap size (Oy direction) and its pole area (xOz plane), the excitation current (amper-turns), the (Oz) distance from the cell to the permanent magnets, the spacing (Ox) between the permanent magnets, their volumes, remanent magnetization (Fig. 2).

The MBs used to intercept the biomarkers are superparamagnetic iron oxide particles (SPIONs), a multipurpose class of agents. They are used in magnetic drug targeting and as magnetic fluid hyperthermia treatment for cancers [16], antimicrobial applications [17], or clinical uses such as in the detection of hepatocellular carcinomas [18].

MB with smaller diameters (500 nm, 200 nm, and 100 nm) were tested in the preliminary steps of assay development [6]. It was observed that they must outnumber the cells to give a spectrometric measurable signal, which may result in clustering without a target analyte (we conjecture by a magnetic effect), thus showing false positive results. Effective capturing yield and high spectrometric response were noticed for 1 μm and 2.7 μm MB. MBs larger than 1–3 μm were considered unsuitable as nonspecific clustering or clogging could occur. The optimization study on the MBs' number and size led to $5 \cdot 10^4$ 2.7 μm MBs.

The MBs get magnetized within an external magnetic field, which may act upon them (body forces and torques) to shape them in a cloudy, aggregate-like structure.

The MBs comprise a superparamagnetic core covered by a uniformly thick ligand layer (shell) for binding the targeted cells from the analyte sample (Fig. 3).

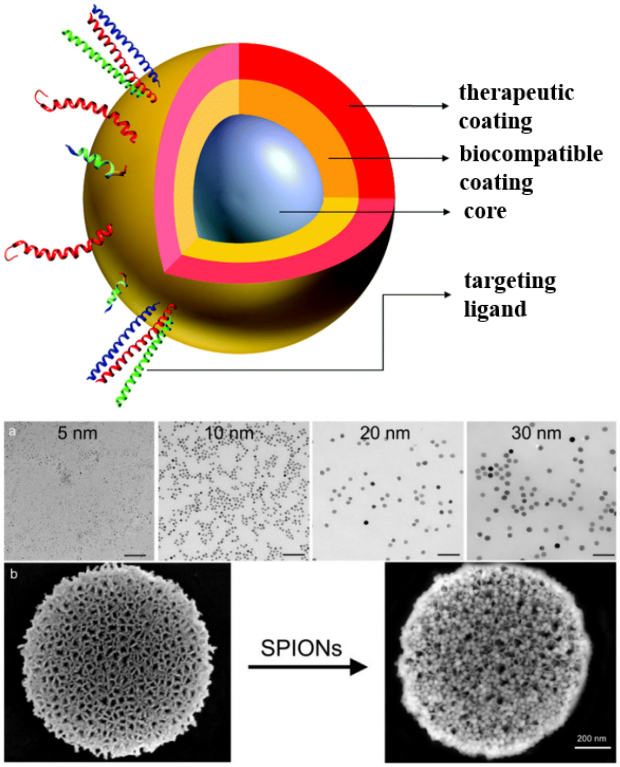

Fig. 3 – SPION structure (above) [19], microscope images for single particles of different sizes, and a SPION matrix created using porous silicon (below) [20].

We are concerned with three parameters of the magnetic actuation system: (1) the coil excitation (amper-turns), (2) the remanent magnetic flux density of the permanent magnets, and (3) the distance between the magnets and the recipient containing the analyte sample (*mag_dist*, Fig. 2). The magnetic force acts on the magnetizable aggregate for different positions inside the cell, which makes the object of this study. The dynamics of the magnetic (driving) and fluidic (opposing) forces make the object of future work, as is the spectroscopy part of the analysis. The stirring process

is assumed to be isothermal, and the different properties are taken at the lab temperature of 20 °C.

Although the magnetic stirring process is dynamic, we consider only several remarkable instants here, for the MB cloud at the margins of the cell (by the poles) and in the middle of the cell (*MB_dist*, Fig. 2).

3. THE MODEL DESCRIPTION

The size and number of the MB clusters depend only on the number of the recipient bacteria in the cell [6] and are exclusively owing to immuno-binding. MB clustering does not happen in the absence of target cells nor in the presence of other nonspecific cells.

MB clusters' "cloud" oscillates between the electrodes when switching the electromagnet's polarity [6], assuming that the MB cloud behaves as an aggregate body is reasonable for a first-level analysis. The MBs' ligand coating and the fluid environment in which they are initially distributed are assumed to result in a compact, porous, saturated medium whose pores do not communicate.

This aggregate's properties may be quantified using a volume-weighted homogenization approach.

Table 1 presents the control parameters of the beads used in the apparatus.

Table 1

Dynabeads M-280 Streptavidin – quality parameters [21]

Parameter	Method	Requirement
Particle concentration	Dry weight measurement of beads	9.7 – 10.5 mg/ml
Functional assay	Tested for free biotin binding capacity	400 – 750 pmol free biotin bound per mg coated beads

The currents' sense in the electromagnet's coils is switched periodically, Fig. 4. There is no time interval between switching.

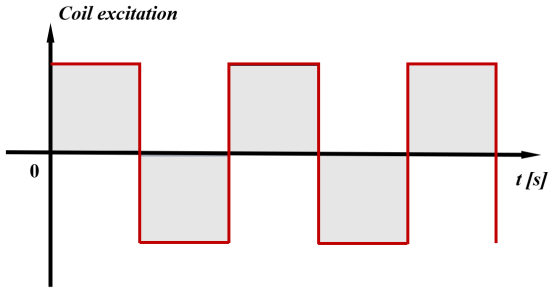

Fig. 4 – The electric current excitation of the coils – the duty factor is 0.5, the period is 0.5 s .

Instead of the dynamics analysis of the aggregate displacement inside the cell, we consider only several snapshots (time instants) for the aggregate – the middle and the margins of the containing recipient. The following equations describe the underlying magnetic field's stationary state,

in the air

$$\nabla \times \left(\frac{1}{\mu_0} \cdot \nabla \times \mathbf{A}\right) = 0, \tag{1}$$

in the permanent magnets

$$\nabla \times \left(\frac{1}{\mu_0 \cdot \mu_{r,mag}} \cdot \nabla \times \mathbf{A} - \mathbf{M}_{mag}\right) = 0, \tag{2}$$

in the magnetizable aggregate

$$\nabla \times \left(\frac{1}{\mu_0 \cdot \mu_{r,MB}} \cdot \nabla \times \mathbf{A} - \mathbf{M}_{MB}\right) = 0, \tag{3}$$

in the magnetic yoke

$$\nabla \times \left(\frac{1}{\mu_0 \cdot \mu_{r,yoke}} \cdot \nabla \times \mathbf{A}\right) = 0, \tag{4}$$

in the coils

$$\nabla \times \left(\frac{1}{\mu_0 \cdot \mu_{r,coil}} \cdot \nabla \times \mathbf{A}\right) = \mathbf{J}, \tag{5}$$

where **A** [Wb/m] is the magnetic vector potential introduced by the divergence-free gauge condition

$$\mathbf{B} = \nabla \times \mathbf{A}, \tag{6}$$

$$\nabla \cdot \mathbf{A} = 0, \tag{7}$$

B [T] is the magnetic flux density, μ_0 is the magnetic permeability of vacuum, $\mu_{r,mag}$ is the relative magnetic permeability of the permanent magnets, $\mu_{r,MB}$ (1.3) is the relative magnetic permeability of the aggregate, $\mu_{r,yoke}$ is the relative magnetic permeability of the electromagnet's soft iron yoke, $\mu_{r,coil}$ is the relative magnetic permeability of the copper coils, $\mathbf{M}_{mag}$ is the magnetization for the permanent magnets, $\mathbf{M}_{MB}$ is the magnetization for the magnetizable aggregate, and **J** [A/m^2] is the electric current density that gives the coils' excitation.

The total magnetization force $\mathbf{F}_{mg}$ that acts upon the aggregate is given by

$$\mathbf{F}_{mg} = (\mathbf{M} \cdot \nabla)\mathbf{H} \tag{8}$$

where **H** [A/m] is the magnetic field strength.

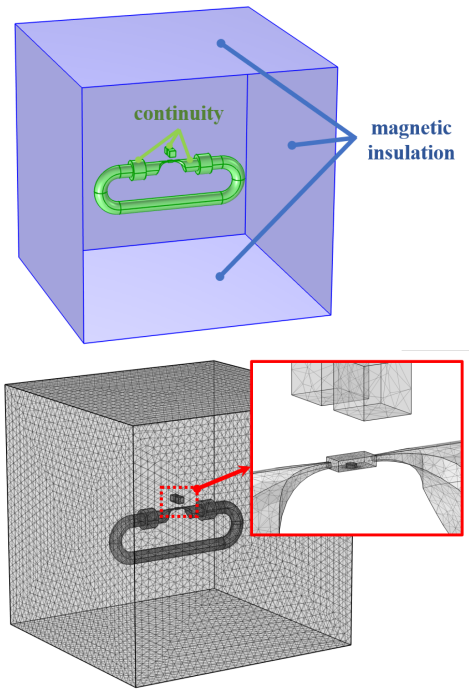

Fig. 5 – The computational domain, enclosing boundary conditions (above), and the mesh comprised approximately 560.500 tetrahedral, Lagrange elements (below).

The parallelepipedic imaginary box enclosing the apparatus (Fig. 5) is sized to contain the magnetic field fully. Its faces define the boundary on which magnetic insulation conditions are set ($\mathbf{n} \times \mathbf{A} = 0$). A similar mathematical model

is used in [22–24] to numerically evaluate the magnetic field.

The electromagnet comprises two solenoid coils fixed on a magnetic yoke made of soft iron material, with $\mu_{r,yoke}$ = 4000 in its linear region. The magnetic field strength produced by the coils' currents provides (magnetic) linear working conditions for the magnetic circuit (including the magnetizable aggregate inside the cell).

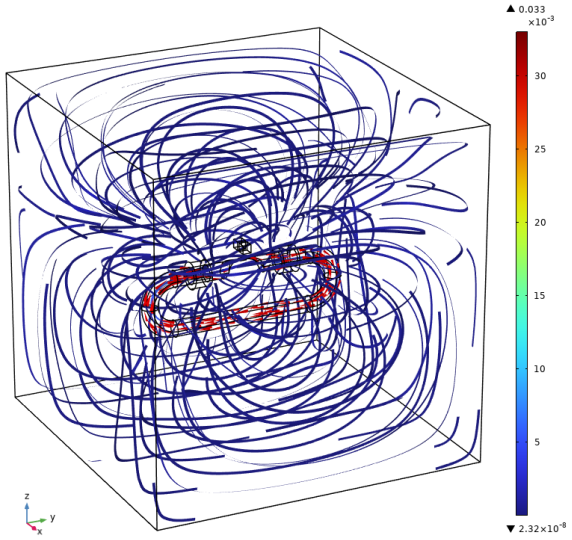

Fig. 6 – The magnetic flux density generated by the two solenoidal coils sharing the same magnetic yoke.

The cylindrical coils are identical and made of copper wire (max. current density $J_0 = 5 \cdot 10^5$ A/m^2). They are powered simultaneously, and their magnetic fields are in the same direction, Fig. 6.

The cubic magnets have a 5 mm edge, a remanent magnetic flux density of 1.3 T, the relative magnetic permeability $\mu_{r,mag} = 10$, and the magnetic poles oriented as presented in Fig. 1. The xOz symmetry planes of the magnets and that of the cell coincide. The magnets are positioned 5 mm above the magnetic yoke (*mag_dist*, Fig. 2). The magnetic field produced by the permanent magnets is presented in Fig. 7.

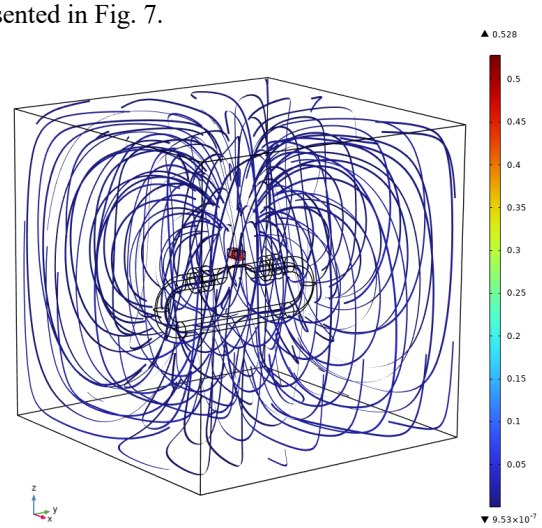

Fig. 7 – The magnetic flux density generated by the permanent magnets – units are Tesla.

Figure 8 shows the total magnetic flux density produced by the electromagnets and the permanent magnets together (Fig. 8, a) and the magnetization forces $\mathbf{F}_{mg}$ acting on the aggregate (Fig. 8, b), evaluated using eq. (8). The magnetic field given by the permanent magnets dominates, as its peak value is four orders of magnitude greater than the peak of the magnetic field produced by the electromagnet. The magnetic yoke's geometry is considerably narrowed at both ends, acting as a magnetic flux concentrator for the region of interest – the sample recipient.

The magnetic force generated by the permanent magnets provides the lifting force that makes the MB float in the sample's volume, thus eliminating the friction forces that could occur if the MBs were moving in direct contact with the recipient's walls. Conversely, the electromagnet generates a magnetic force necessary to make the MBs move inside the recipient and efficiently capture the targeted pathogenic cells in the sample. The total magnetization forces that act upon the magnetizable aggregate are depicted in Fig. 8, b.

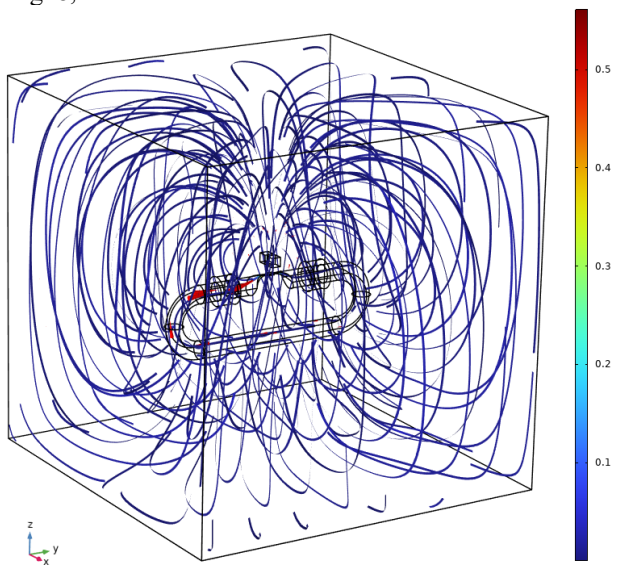

(a)

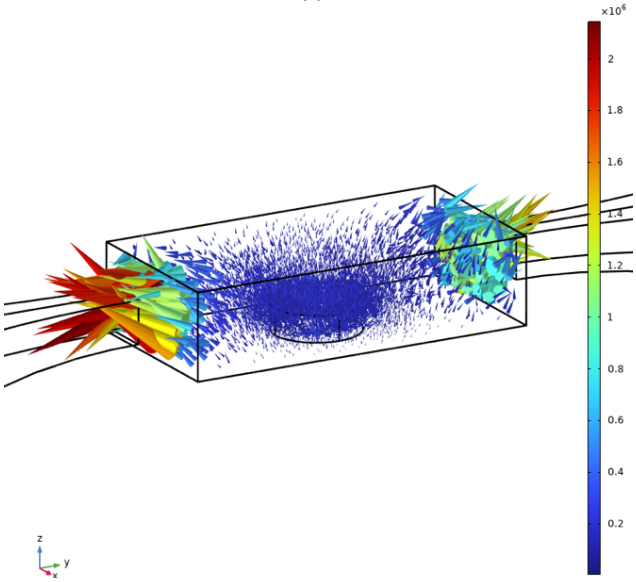

(b)

Fig. 8 – The magnetic flux density produced by the magnetic actuation system: (a) and the magnetization force upon the magnetizable aggregate (b).

4. NUMERICAL SIMULATION RESULTS AND DISCUSSION

The underlying magnetic field is seen through magnetic flux density lines in Fig. 8, a. The flux tube is concentrated by the

poles at the cell level, where the magnetic flux reaches 0.5 T.

Thus, the optimal actuation frequency of 2 Hz was chosen, allowing a measurable signal for simple MBs, and distinguishing between unbound MB and MB clusters.

CASE 1 – PARAMETRIC STUDY: COILS EXCITATION

In this case, the excitation of the coil was parametrized, while the permanent magnets' distance from the sample (*mag_dist* = 5 mm) and its remanent flux density of $\mathbf{B}_{rem}$ = 1.3 T were kept constant. The total magnetization force $\mathbf{F}_{mg}$ was evaluated using eq. (8) for the MB cluster. The magnetizable aggregate is assumed to be a small disc inside the sample recipient at three locations (*MB_dist*, Fig. 2): left extreme, center, and right margin.

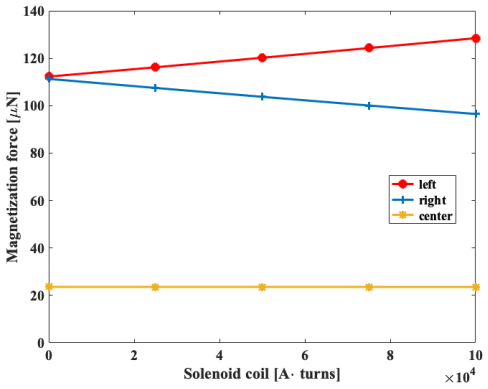

Fig. 9 – Magnetization force that acts upon the magnetizable aggregate for different coil excitation values.

The results in Fig. 9 show that the total magnetization force decreases primarily when the cluster reaches the recipient's center (farthest from the electromagnet's ends).

CASE 2 – PARAMETRIC STUDY: REMANENT FLUX DENSITY OF THE PERMANENT MAGNETS

In this second case, the coil excitation (maximum value) and the permanent magnets' distance from the sample (*mag_dist* = 5 mm) were kept the same. In contrast, the remanent magnetic flux density of the permanent magnets $\mathbf{B}_{rem}$ was parametrized, and the total magnetization force $\mathbf{F}_{mg}$ upon the MB cluster was calculated.

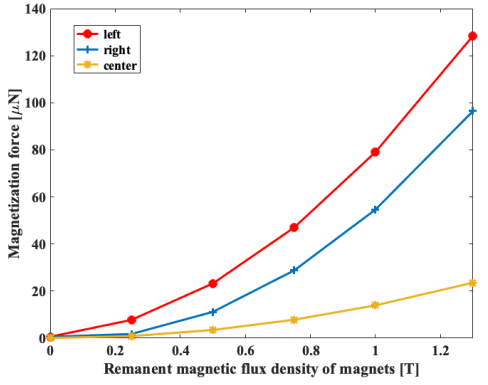

Fig. 10 – Magnetization force that acts upon the magnetizable aggregate for different remanent magnetic flux density values.

As expected, the total magnetization force increases for stronger permanent magnets.

CASE 3 – PARAMETRIC STUDY: THE DISTANCE FROM MAGNETS TO CELL

The third case presents the results when modifying the magnets–sample recipient distance (*mag_dist*) while the remanent magnetic flux density and the coil excitation are at their peak values.

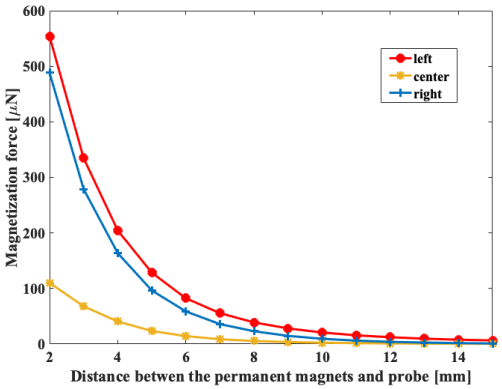

Fig. 11 – Magnetization force that acts upon the magnetizable aggregate for different magnets – sample recipient distance values.

The total magnetization force in the cluster decreases noticeably when the magnets are placed farther from the region of interest. For *MB_dist* greater than 8 mm, the influence of the permanent magnets tends towards zero value, which means that no lifting force will act upon the MBs, and their dynamics will sensibly change.

5. CONCLUSIONS

The paper presents numerical analysis results for efficiently controlling and fine-tuning the magnetic field in a conceptual pathogenic bacteria detection platform based on a hybrid solution comprised of two magnetic field sources: a pair of strong permanent magnets and an electromagnet made of two solenoid coils that share the same magnetic yoke.

The numerical results outline the complex magnetic field spectrum of the system and the magnetization forces exerted upon the magnetizable aggregate. One geometrical parameter (the magnets – sample recipient distance) and two other system parameters (coil excitation and remanent magnetic flux density) were varied to predict their influence upon the total magnetization forces influencing the MBs dynamics and behavior in the targeted pathogenic cell binding process.

The magnetic field of the PM is highly non-uniform. Its structure depends on several concurring geometric parameters that, in principle, could be adjusted continuously using ancillary fine mechanics extensions. However, its $\mathbf{B}_{rem}$ is not "adjustable" in a specific layout. Thus, tuning the PM source as an ensemble to reach an optimum action upon the aggregate may be difficult. Here, we were concerned with a limited range of numerical experiments to prove the PM usage efficiency.

And efficient the PM is: it enhances the non-uniformity of the total magnetic field (the more non-uniform it is, the larger the magnetic body forces are) and provides for a lifting force that may reduce the friction between the aggregate and the boundary layer at cell bottom (the "immersion" fluid is viscous), should the aggregate touch it. Some means to prevent the aggregate extraction from the cell should be taken (*e.g.*, an upper lid for the compartment).

ACKNOWLEDGEMENTS

The work was conducted in the Laboratory for Multiphysics Modeling at the National University for Science and Technology Politehnica of Bucharest. The second author acknowledges the funding through the

Ministry of Investments and European Projects through the Human Capital Sectoral Operational Program 2014-2020, Contract no. 62461/03.06.2022, SMIS code 153735, and the outstanding support provided by the International Centre of Biodynamics.

Received on 18 September 2023

REFERENCES

1. Y. Zhu, Y. Zhang, X. Yang, S. Tao, M. Chen, W. Shangguan, *Operando investigation of particle re-entrainment mechanism in electrostatic capture process on the lab-on-a-chip*, Journal of environmental sciences, **136**, pp. 337–347 (2024).
2. L. Steigmann, S. Maekawa, C. Sima, S. Travan, C.-W. Wang, W.V. Giannobile, *Biosensor and Lab-on-a-chip Biomarker-identifying Technologies for Oral and Periodontal Diseases*, Front. Pharmacol. **11** p. 1663 (2020).
3. Y. Ai, F. Zhang, C. Wang, R. Xie, Q. Liang, *Recent progress in lab-on-a-chip for pharmaceutical analysis and pharmacological/toxicological test*, Trends in Analytical Chemistry, **117**, pp. 215-230 (2019).
4. A. M. Foudeh, T. Fatanat Didar, T. Veres and M. Tabrizian, *Lab Chip*, **12**, pp. 3249–3266 (2012).
5. H.S. Magar, M.N. Abbas, M.B. Ali, M.A. Ahmed, *Picomolar-sensitive impedimetric sensor for salivary calcium analysis at POC based on SAM of Schiff base–modified gold electrode*. J. Solid State Electrochem., **24**, pp. 723–737 (2020).
6. S. David, C. Polonschii, M. Gheorghiu, D. Bratu, A. Dobre, E. Gheorghiu, *Assessment of pathogenic bacteria using periodic actuation*, Lab on a Chip, **13**, p. 3192 (2013).
7 E. Gheorghiu, *Detection of pathogenic bacteria by magneto-immunoassays: a review*. The Journal of Biomedical Research. **35**. 1. 10.7555/JBR.34.20200123 (2021).
8 F. Munteanu, A.M. Titoiu, J. Marty, A. Vasilescu, *Detection of Antibiotics and Evaluation of Antibacterial Activity with Screen-Printed Electrodes*. Sensors. **18**. 901. 10.3390/s18030901 (2018).
9. P.H. Lu, Y.D. Ma, C.Y. Fu, G.B. Lee, *A structure-free digital microfluidic platform for detection of influenza a virus by using magnetic beads and electromagnetic forces*. Lab on a Chip, **4**, pp.789–797 (2020).
10. A.F. Blanco, M. Hernandez Perez, Y. Moreno Trigos, J. Garcia-Hernandez, *Development of Optical Label-Free Biosensor Method in Detection of Listeria monocytogenes from Food*. Sensors. **23**. 5570. 10.3390/s23125570 (2023).
11. R. Radhakrishnan, P. Poltronieri, *Fluorescence-Free Biosensor Methods in Detection of Food Pathogens with a Special Focus on Listeria monocytogenes*. Biosensors, MDPI, ISSN 2079-6374;. **7**. 63. 10.3390/bios7040063 (2017)
12. J. Leva-Bueno, S.A. Peyman, P.A. Millner, *A review on impedimetric immunosensors for pathogen and biomarker detection,* Med Microbiol Immunol, **209**, *3*, pp. 343–362 (2020).
13. J. Vlcek, Pištora, M. Lesnák, *Design of plasmonic-waveguiding structures for sensor applications*, Nanomaterials, **9**, *9*, pp. 1227 (2019).
14. E. Gheorghiu*, A renewed challenge to electrical bioimpedance: rapid assessment of pathogenic bacteria*, J. Electr. Bioimpedance, **14**, *1*, pp. 1-2 (Mar. 2023).
15. E. Gheorghiu*, RO Patent Application* A00136/2011 (2011).
16. A.M. Morega, M. Morega, A.A. Dobre, *Computational Modeling in Biomedical Engineering and Medical Physics*, Chapters 6 and 8 Elsevier, (2020).
17. A.B. Seabra et al., *Chapter 24, Antimicrobial applications of superparamagnetic iron oxide nanoparticles: perspectives and challenges*, in *Nanostructures for Antimicrobial Therapy*, ed. A. A. Ficai, A.M. Grumezescu, *Micro and Nano Technologies*, pp. 531-550 (2017).
18. J. Dulińska-Litewka et al*., Superparamagnetic iron oxide nanoparticles – current and prospective medical applications*, Materials (Basel), **12**, *4*, pp. 617-642 (2019).
19. S. Palanisamy Y.M. Wang, *Superparamagnetic iron oxide nanoparticulate system: synthesis, targeting, drug delivery and therapy in cancer*, Dalton Transactions, **48**, *26*, pp. 9490-9515 (2019).
20. C.M. Lundquist et al., *Characterization of Free and Porous Silicon-Encapsulated Superparamagnetic Iron Oxide Nanoparticles as Platforms for the Development of Theranostic Vaccines*, Med. Sci., **2**, *1*, pp. 51-69 (2014).
21. ***ThermoFisher Invitrogen Dynabeads M-280 Streptavidin Certificate of Analysis, *Quality Control Report*, September 2023, https://www.thermofisher.com/document-connect/document-connect.html?url=https://assets.thermofisher.com/TFS-Assets%2Fcertificate%2FVIL%2FCOA%2FCOA_60210_2812162_1.pdf.
22. A.M. Morega, M.Morega, J.B. Dumitru, *Magnetic field-flow interactions in a miniature electric power transformer with magnetic nanofluid core and solenoid type coils*, Rev. Roum. Sci. Techn. – Électrotechn. Et Énerg., **58**, *1*, pp. 25–34 (2013).
23. V. Paltanea, G. Paltanea, D. Popovici, *Numerical approach for an application of magnetic drug targeting in cancer therapy*, Rev. Roum. Sci. Techn. – Électrotechn. Et Énerg., **53**, *2*, pp. 137–146 (2008).
24. R.M. Baerov, A.M. Morega, M. Morega, *Analysis of magnetotherapy effects for post-traumatic recovery of limb fractures*, Rev. Roum. Sci. Techn. – Électrotechn. Et Énerg., **65**, *1-2*, pp. 145–150 (2020).